THE JOURNAL OF BIOLOGICAL CHEMISTRY VOL. 291, NO. 21, pp. 11003–11015, May 20, 2016
Published in the U.S.A.

PilN Binding Modulates the Structure and Binding Partners of the *Pseudomonas aeruginosa* Type IVa Pilus Protein PilM*[S]

Received for publication, January 28, 2016, and in revised form, March 9, 2016 Published, JBC Papers in Press, March 28, 2016, DOI 10.1074/jbc.M116.718353

Matthew McCallum[‡§1], Stephanie Tammam[§], Dustin J. Little[‡§2], Howard Robinson[¶], Jason Koo[§], Megha Shah[‡], Charles Calmettes[‡], Trevor F. Moraes[‡], Lori L. Burrows[‖3], and P. Lynne Howell[‡§4]

From the [‡]Department of Biochemistry, University of Toronto, Toronto, Ontario M5S 1A8, Canada, the [§]Program in Molecular Structure and Function, Peter Gilgan Centre for Research and Learning, Hospital for Sick Children, Toronto, Ontario M5G 0A4, Canada, the [¶]Photon Sciences Division, Brookhaven National Laboratory, Upton, New York 11973-5000, and the [‖]Department of Biochemistry and Biomedical Sciences and the Michael G. DeGroote Institute for Infectious Disease Research, McMaster University, Hamilton, Ontario L8N 3Z5, Canada

Pseudomonas aeruginosa **is an opportunistic bacterial pathogen that expresses type IVa pili. The pilus assembly system, which promotes surface-associated twitching motility and virulence, is composed of inner and outer membrane subcomplexes, connected by an alignment subcomplex composed of PilMNOP. PilM binds to the N terminus of PilN, and we hypothesize that this interaction causes functionally significant structural changes in PilM. To characterize this interaction, we determined the crystal structures of PilM and a PilM chimera where PilM was fused to the first 12 residues of PilN (PilM·PilN(1–12)). Structural analysis, multiangle light scattering coupled with size exclusion chromatography, and bacterial two-hybrid data revealed that PilM forms dimers mediated by the binding of a novel conserved motif in the N terminus of PilM, and binding PilN abrogates this binding interface, resulting in PilM monomerization. Structural comparison of PilM with PilM·PilN(1–12) revealed that upon PilN binding, there is a large domain closure in PilM that alters its ATP binding site. Using biolayer interferometry, we found that the association rate of PilN with PilM is higher in the presence of ATP compared with ADP. Bacterial two-hybrid data suggested the connectivity of the cytoplasmic and inner membrane components of the type IVa pilus machinery in *P. aeruginosa*, with PilM binding to PilB, PilT, and PilC in addition to PilN. Pull-down experiments demonstrated direct interactions of PilM with PilB and PilT. We propose a working model in which dynamic binding of PilN facilitates functionally relevant structural changes in PilM.**

Type IVa pili (T4aP)[5] are hairlike protein filaments critical for initial and irreversible bacterial attachment, pro-biofilm cyclic diguanylate signaling, spatial differentiation in biofilms, the dispersal of mature biofilms, swarming motility, twitching motility, competence for DNA uptake, and pathogenesis in *Pseudomonas aeruginosa* (1–6). After decades of research, many of the essential *P. aeruginosa* T4aP proteins have been characterized (7–9) (Fig. 1). The pilus fiber is composed predominantly of the major subunit PilA plus small amounts of minor pilins and is proposed to be assembled and disassembled by the cytoplasmic motor subcomplex, composed of the inner membrane protein PilC and orthologous AAA+ ATPases PilB, PilT, and PilU (9). PilB and PilT power assembly and disassembly, respectively (10–12). The exact function of PilU remains unclear. The pilus extends through a multimeric outer membrane PilQ secretin (6, 13). PilQ interacts with PilP, which in turn interacts with PilNO heterodimers (14). In the cytoplasm, PilM associates with this complex by binding the conserved cytoplasmic N terminus of PilN (14, 15), although PilM is not dependent on PilN, PilO, or PilP for stability (16). Little is known of the exact molecular function of PilM, but Δ*pilM* mutants lack T4aP (16–23).

The structure of PilM bound to a peptide corresponding to the first 15 N-terminal residues of PilN from *Thermus thermophilus* was solved previously, revealing that PilM is an actin homolog with structural similarities to BfpC, GspL, and FtsA (15, 24). GspL and BfpC are components of the type II secretion (T2S) and type IVb pilus (T4bP) systems, respectively. These systems share evolutionary origins with the T4aP because they

* This work was supported in part by Canadian Institutes for Health Research (CIHR) Grant MOP 93585 (to L. L. B. and P. L. H.). The authors declare that they have no conflicts of interest with the contents of this article. The content is solely the responsibility of the authors and does not necessarily represent the official views of the National Institutes of Health.

[S] This article contains supplemental Animations 1 and 2.

The atomic coordinates and structure factors (codes 5EOX, 5EOY, 5EOU, and 5EQ6) have been deposited in the Protein Data Bank (http://wwpdb.org/).

[1] Supported by a CIHR doctoral studentship.

[2] Supported in part by graduate scholarships from the University of Toronto, the Ontario Graduate Scholarship Program, and CIHR.

[3] To whom correspondence may be addressed: Dept. of Biochemistry and Biomedical Sciences and the Michael G. DeGroote Institute for Infectious Disease Research, McMaster University, Hamilton, Ontario L8N 3Z5, Canada. E-mail: burrowl@mcmaster.ca.

[4] Recipient of a Canada Research Chair. To whom correspondence may be addressed: Program in Molecular Structure and Function, Peter Gilgan Centre for Research and Learning, Hospital for Sick Children, 686 Bay St., Toronto, Ontario M5G 0A4, Canada. E-mail: howell@sickkids.ca.

[5] The abbreviations used are: T4aP, type IVa pilus/pili; T2S, type II secretion; T4bP, type IVb pilus/pili; SEC, size exclusion chromatography; MALS, multiangle light scattering; BACTH, bacterial two-hybrid; $RMSD_{C\alpha}$, root mean square deviation of Cα atomic coordinates; AMP-PNP, adenylyl-imidodiphosphate; ITC, isothermal titration calorimetry; SeMet, selenomethionine; Ni-NTA, nickel-nitrilotriacetic acid; CV, column volumes; BisTris, 2-[bis(2-hydroxyethyl)amino]-2-(hydroxymethyl)propane-1,3-diol; PDB, Protein Data Bank.

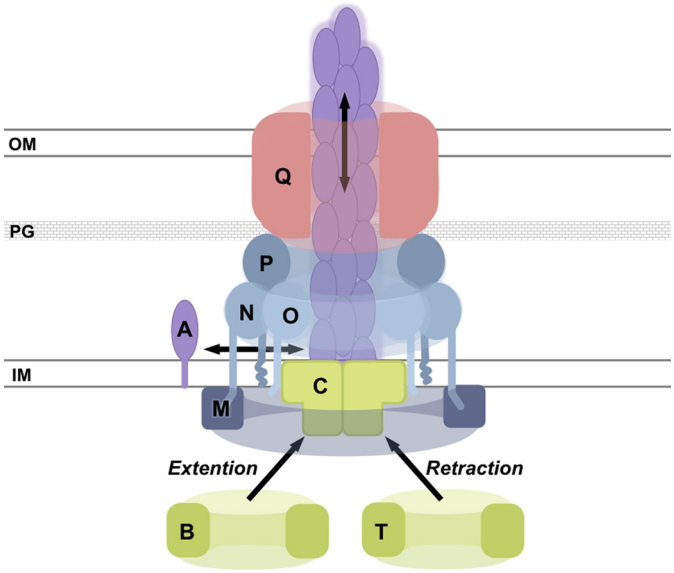

FIGURE 1. **Schematic model of selected type IV pilus assembly machinery components.** PilA assembly into a pilus fiber is referred to as pilus extension, whereas PilA fiber disassembly is referred to as pilus retraction. PilB has been implicated in pilus extension, whereas PilT is thought to be involved in pilus retraction. The schematic is not to scale. *OM*, outer membrane; *PG*, peptidoglycan; *IM*, inner membrane. The *single letters* represent protein names (*e.g.* PilM (*M*)).

are structurally and functionally related (8, 9). GspL and BfpC are bitopic membrane proteins that appear to be the functional equivalents of PilM and PilN. GspL and BfpC bind to and activate their PilB equivalents (24–27) and bind PilC equivalents (24, 27). These data suggest that PilM may bind PilB and/or PilC. However, GspL and BfpC deviate substantially from PilM. These proteins are more than 100 residues shorter and consequently lack the ability to bind ATP (28), thereby limiting the extent to which we can generate testable hypotheses for PilM based on the structures of GspL and BfpC.

Despite the similarities among the T4aP, T4bP, and T2S systems, PilM is structurally more similar to FtsA, a key component of the bacterial divisome (15). FtsA forms polymers that can be visualized by negative stain electron microscopy and as a consequence of the packing interactions in FtsA crystal structures (29, 30). FtsA binds to FtsN, and this interaction is thought to lead to dissociation of the FtsA polymers, exposing protein-binding sites that allow for recruitment and activation of downstream cell division proteins (31–33). PilN and FtsN share 14% sequence identity (28% similarity) and have similar topology, including conserved cytoplasmic N-terminal residues (32), a single transmembrane helix, and a structurally similar circularly permutated $\beta\alpha\beta\beta(\alpha\beta)$ ferredoxin-like fold ($RMSD_{C\alpha}$ = 1.9 Å over 43 residues, PDB codes 1UTA and 4BHQ). Furthermore, identification of key residues involved in the FtsN-FtsA interaction suggests that FtsA binds FtsN using a binding pocket analogous to that used by PilM to bind PilN (33). Similar comparisons have been made elsewhere (32, 34), leading us to hypothesize that binding of PilN to PilM causes structural changes in PilM that dictate the nature of its binding partners.

Herein we describe the structures of PilM and of PilM C-terminally linked to the first 12 residues of PilN (PilM·PilN(1–12)). Crystallographic and functional characterization revealed that PilM binds its own N terminus to form a dimer and that binding of ATP facilitates PilN binding. The binding of PilN was found to cause long range conformational changes and to lead to PilM monomerization. Furthermore, we show that PilM binds to PilB, PilT, and possibly PilC and that binding of PilN may modulate the interaction of PilM with PilB, PilT, and/or PilC.

Experimental Procedures

Primers, Strains, and Plasmids—The primers, strains, and plasmids used in this study are listed in Table 1.

Cloning, Expression, and Purification of PilM, PilB, and PilT—Cloning of PilM, PilB, and PilT into pET28a with a thrombin-cleavable hexahistadine tag was described previously (10). pET28a:PilM was further modified by round-the-horn PCR mutagenesis using primers P1 and P2 to generate pET28a:PilM·PilN(1–12) (PilM C-terminally fused to the first 12 residues of PilN with a 3-residue linker) and primers P11 and P51 to generate pET28a:PilM$^{\Delta 2-8}$ (Table 1). pET28a:PilM was also mutated by site-directed mutagenesis to generate pET28a:PilM^{K52A} using primers P13 and P14 and pET28a:PilM^{S19A} using primers P17 and P18. The fidelity of the sequences was verified by TCAG sequencing facilities (Hospital for Sick Children). *Escherichia coli* BL21-CodonPlus® cells (Stratagene) transformed with pET28a:PilM, pET28a:PilM·PilN(1–12), pET28a:PilM$^{\Delta 2-8}$, and pET28a:PilT and *E. coli* C41(DE3) transformed with pET28a:PilB were grown in 4 liters of lysogeny broth (LB) with 100 μg/ml kanamycin and 1% (w/v) glucose at 37 °C to an A_{600} of 0.5–0.6, and then protein expression was induced by the addition of isopropyl-D-1-thiogalactopyranoside to a final concentration of 1 mM, and the cells were grown for 16 h at 18 °C. For production of selenomethionine (SeMet)-incorporated PilM, pET28a:PilM was transformed into *E. coli* B834 Met$^-$ (Novagen) and expressed as described elsewhere (35). Cells were pelleted by centrifugation at 9000 × *g* for 20 min.

For PilM and PilM·PilN(1–12), cell pellets were subsequently resuspended in 30 ml of buffer A1 (50 mM Tris, pH 7.0, 150 mM NaCl, 30 mM citrate, 10% (v/v) glycerol, 2 mM tris(2-carboxyethyl)phosphine, 5 mM $MgCl_2$, 5 mM ATP, and 50 mM imidazole). ATP was omitted when PilM was used in the ATPase assays. Resuspended cells were lysed by passage through an Emulsiflex-c3 high pressure homogenizer, and the cell debris was removed by centrifugation for 30 min at 40,000 × *g*. The resulting supernatant was passed over a column containing 5 ml of pre-equilibrated Ni-NTA-agarose resin (Life Technologies, Inc.). The resin was first washed with 10 column volumes (CV) of buffer A1 and then 10 CV of buffer A2 (buffer A1 adjusted to pH 6.0) before elution with 5 ml of buffer A2 plus 300 mM imidazole. The protein was then further purified by size exclusion chromatography on a HiLoad™ 16/600 Superdex™ 200pg column pre-equilibrated with buffer A2 without ATP or imidazole. Purified PilM constructs, with the exception of PilM$^{\Delta 2-8}$, which precipitated at room temperature, were treated with thrombin (EMD Millipore) for 16 h at room temperature and separated from the tagged protein using a second round of nickel affinity purification.

TABLE 1
Primers, strains, and plasmids used in this study

Primers	Sequence	Reference
P1	CCTGCTGCCGTGGCGCGAAGAATGAGAGCACCAC CACCACCAC	This Study
P2	TTAATGCGCGCCATGCCGCTGCTGTCGAAACTCCT CAACGCCAG	This Study
P11	ACCTTGCTGGGGATCGA	This Study
P51	TAGCATATGGCTGCCGC	This Study
P17	CTTTACCGAGGTCGCGCTGATGTCGATCCC	This Study
P18	GGGATCGACATCAGCGCGACCTCGGTAAAG	This Study
P13	AGCTCGACGATGTTCGCTTCCACGACTGCATT	This Study
P14	AATGCAGTCGTGGAAGCGAACATCGTCGAGCT	This Study
PilU_F	GCGTCTAGAGATGGAATTCGAAAAGCTGCTGC	This Study
PilU_R	GCGGGTACCGCTGGCCTACTGAAGACGGT	This Study
PilT_F	GCGTCTAGAGATGGATATTACCGAGCTGCTCG	This Study
PilT_R	GCGGGTACCTCAGAAGTTTTCCGGGATCTTC	This Study
PilMN1-12_F	TATATATATCTAGAGGTGCTAGGGCTCATAAAGAA GAAA	This Study
PilMN1-12_R	TATATATAGAATTCGTCACCAGGGTAGAAGGTTGA TCCGTGCCATGTCGAAACTCC	This Study
PilB_F	TATATATATCTAGAGATGAACGACAGCATCCAACT G	This Study
PilB_R	TATATATAGAATTCGTTAATCCTTGGTCACGCGGTT	This Study
PilC_F	TATATAACTCTAGAGATGGCGGACAAAGCGTTAAA AACCAG	This Study
PilC_R	TATATATGGAATTCGTTATCCGACGACGTTGCCGA G	This Study
PilA_F	GCGTCTAGAACTGATGAAAGCTCAAAAAGGCTTTA C	This Study
PilA_R	CATGAGCTCTCTGTTATCACAACCTTTCGGAGTG	This Study

Strains	Description	Reference
E. coli DH5α	Cloning strain; F^-, *endA1*, *glnV44*, *thi-1*, *recA1*, *relA1*, *gyrA96*, *deoR*, *nupG*, *purB20*, φ80d*lacZ*ΔM15, Δ(*lacZYA-argF*), U169, *hsdR17*($r_K^-m_K^+$), λ^-	Invitrogen
E. coli TOP10	F^-, mcrA Δ(mrr-hsdRMS-mcrBC) φ80lacZΔM15 ΔlacX74 nupG recA1 araD139 Δ(ara-leu)7697 galE15 galK16 rpsL(Str^R) endA1 λ^-	Invitrogen
E. coli C41	Expression strain; F^-, *ompT*, *gal, dcm, hsdS*$_B$($r_B^-m_B^-$), (DE3)	Sigma
E. coli BL21-CodonPlus® cells	Expression strain; F^- *ompT hsdS* (rB^-mB^-) dcm^+ Tet^r galλ (DE3) endA [*argU proL* Cam^r]	Stratagene
E. coli B834	Expression strain; F^- *ompT hsdS*$_B$ (rB^-mB^-) *gal dcm met* (DE3)	Novagen
E. coli BTH101	BACTH coexpression strain; F^-, *cya-99, araD139, galE15, galK16, rpsL1*, *hsdR2, mcrA1, mcrB1*	Euromex
P. aeruginosa PAO1	Wildtype template for cloning.	ATCC

Plasmids	Description	Reference
pET28a::PilB	PilB expression	(10)
pET28a::PilT	PilT expression	(10)
pET28a::PilM	PilM expression	(14)
pET28a::PilM^{K52A}	PilM K52A expression	This Study
pET28a::PilM^{S19A}	PilM S19A expression	This Study
pET28a::PilM:PilN$_{1-12}$	PilM:PilN$_{1-12}$ expression	This Study
pUT18C:PilA	PilA BACTH construct	This Study
pUT18C:PilB	PilB BACTH construct	This Study
pUT18C:PilC	PilC BACTH construct	This Study
pUT18C:PilM	PilM BACTH construct	(50)
pUT18C:PilM:PilN$_{1-12}$	PilM:PilN$_{1-12}$ BACTH construct	This Study
pUT18C:PilN	PilN BACTH construct	(50)
pUT18C:PilO	PilO BACTH construct	(50)
pUT18C:PilT	PilT BACTH construct	This Study
pUT18C:PilU	PilU BACTH construct	This Study
pKT25:PilA	PilA BACTH construct	This Study
pKT25:PilB	PilB BACTH construct	This Study
pKT25:PilC	PilC BACTH construct	This Study
pKT25:PilM	PilM BACTH construct	(50)
pKT25:PilM:PilN$_{1-12}$	PilM:PilN$_{1-12}$ BACTH construct	This Study
pKT25:PilN	PilN BACTH construct	(50)
pKT25:PilO	PilO BACTH construct	(50)
pKT25:PilT	PilT BACTH construct	This Study
pKT25:PilU	PilU BACTH construct	This Study

For the interaction studies between PilM, PilB, and PilT, cell pellets were resuspended in 30 ml of buffer B1 (100 mM Tris, pH 7.0, 150 mM NaCl, 30 mM citrate, 150 mM $(NH_4)_2SO_4$, 15% (v/v) glycerol, 5 mM $MgSO_4$, 50 mM imidazole). Resuspended cells were lysed by passage through an Emulsiflex-c3 high pressure homogenizer, and the insoluble components were pelleted by centrifugation for 60 min at 40,000 × *g*. With the exception of PilB, the resulting supernatant was passed over a column containing 5 ml of pre-equilibrated Ni-NTA-agarose resin (Life Technologies). The Ni-NTA-agarose resin was then washed with 10 CV of buffer B1 and then 10 CV of buffer B2 (200 mM Tris, pH 6.0, 300 mM NaCl, 60 mM citrate, 300 mM $(NH_4)_2SO_4$, 10% (v/v) glycerol, 10 mM $MgSO_4$, and 50 mM imidazole) before adjusting the pH with 10 CV of buffer B3 (buffer B1 adjusted to pH 7.0). The protein was eluted in 5 ml of buffer B3 plus 300 mM imidazole and then further purified by size exclusion chromatography on a HiLoad™ 16/600 Superdex™ 200pg column pre-equilibrated with buffer B3 without imidazole.

For PilB, after the cell pellets were homogenized and centrifuged, insoluble inclusion bodies were solubilized by gentle stirring in 40 ml of buffer B3 plus 8 M urea for 45 min at room temperature. Components that remained insoluble were removed by centrifugation for 30 min at 40,000 × *g*. The resulting supernatant was passed over a HisTrap HP 5-ml (GE Healthcare) nickel affinity column. The resin was washed with 4 CV of buffer B3 plus 8 M urea before elution with a gradient of buffer B3 plus 8 M urea and 300 mM imidazole. Eluted fractions containing PilB were then concentrated to ~12 mg/ml in an ultrafiltration device, and 300 μl were added (in 50-μl increments every minute for 6 min) to 50 ml of gently stirring renaturation buffer (buffer B3 without imidazole plus 5% (v/v) glycerol, 0.5 M arginine, 2 mM tris(2-carboxyethyl)phosphine, and 1 mM ATP) and incubated at 4 °C for 16 h. Then the 50-ml solution was exchanged for buffer B3 without imidazole and concentrated to 500 μl over an ultrafiltration device. The protein was then further purified by size exclusion chromatography on a HiLoad™ 16/600 Superdex™ 200pg column pre-equilibrated with buffer B3 without imidazole. Purified proteins were stored at 4 °C for less than 2 days before use.

Crystallization, Data Collection, and Structure Solution—For crystallization, purified PilM and PilM·PilN(1–12) were concentrated to 15 mg/ml at 3000 × *g* in an ultrafiltration device, and ATP or AMP-PNP (Sigma-Aldrich) was added to a final concentration of 5 mM as detailed below. Crystallization conditions were screened using the complete MCSG suite (MCSG 1–4) (Microlytic), using a Gryphon LCP robot (Art Robbins Instruments). Crystal conditions were screened and optimized using vapor diffusion at 20 °C using Art Robbins Instruments Intelli-Plates (96-3 Shallow Well Hampton Research) with equal amounts of protein and reservoir solution. For PilM, the reservoir solution was 27% (w/v) PEG3350, 0.2 M $MgCl_2$, 0.1 M BisTris, pH 7.0. For PilM·PilN(1–12), the reservoir solution was 2 M $(NH_4)_2SO_4$ and 0.1 M Tris, pH 8.0. The crystals were cryoprotected for 5 s in reservoir solution supplemented with 20% (v/v) ethylene glycol before vitrification in liquid nitrogen. Single wavelength anomalous diffraction or native data, as appropriate, were collected on Beamline X29 at the National Synchrotron Light Source (see Table 2). The data were indexed and scaled using HKL2000 (36). Native data were also collected on PilM with AMP-PNP at the x-ray diffraction facilities at the Hospital for Sick Children on a Bruker D8 Venture machine. These data were indexed and scaled with SAINT (Bruker AXS Inc., Madison, WI). PHENIX Autosol (38) was used to identify the 10 selenium atom positions in the asymmetric unit of SeMet PilM. The resulting electron density map was of high quality and enabled PHENIX AutoBuild (39) to build ~90% of the protein. The remaining residues were built manually in COOT (40). The structures of native PilM and PilM·PilN(1–12) complexed with ATP or AMP-PNP were solved by molecular replacement using the SeMet-PilM struc-

TABLE 2

Data collection and refinement statistics of PilM and PilM:PilN$_{1-12}$ structures

Values in parentheses correspond to the highest resolution shell.

	PilM^{SeMet}·ADP	PilM·ADP	PilM·AMP-PNP	PilM·PilN(1–12)·ATP
Data collection				
Beamline	NSLS X29	NSLS X29	Bruker D8 Venture	NSLS X29
Wavelength (Å)	0.97920	1.0750	1.5406	1.0750
Space group	$P2_12_12$	$P2_12_12$	$P2_12_12$	$P321$
a, *b*, *c* (Å)	110.8, 152.0, 41.6	111.4, 150.4, 41.6	112.6, 151.8, 45.9	131.8, 131.8, 79.0
α, β, γ (degrees)	90.0, 90.0, 90.0	90.0, 90.0, 90.0	90.0, 90.0, 90.0	90.0, 90.0, 120.0
Resolution (Å)	46–2.50 (2.55–2.50)	46–2.40 (2.45–2.40)	20–3.51 (3.63–3.51)	50–2.43 (2.49–2.43)
Total reflections	402,920	406,860	24,279	742,571
Unique reflections	26,503 (1531)	30,127 (1742)	9479 (895)	29,964 (3574)
Redundancy	13.0 (12.9)	11.7 (11.3)	2.6 (1.7)	19.9 (19.8)
Completeness (%)	100 (98)	100 (96)	92 (80)	100 (97)
Mean $I/\sigma I$	18.3 (1.5)	30.6 (1.6)	7.0 (2.9)	21.2 (1.3)
R_{Sym} (%)[a]	11.5 (100)	6.9 (100)	12.9 (26.7)	13.5 (100)
R_{Pim} (%)[a]	4.2 (43.1)	2.5 (41.4)	9.4 (23.2)	4.1 (44.0)
CC* (%)[a]	(92.1)	(92.5)	(88.4)	(93.8)
Refinement				
R_{work}/R_{free} (%)[b]	20.7/26.2	22.4/25.7	24.1/27.4	21.1/23.8
RMSD				
Bond lengths (Å)	0.006	0.005	0.004	0.003
Bond angles (degrees)	0.91	0.86	0.96	0.62
Ramachandran plot[c]		98		
Total favored (%)	98		98	99
Total allowed (%)	100	100	100	100
Coordinate error (Å)[d]	0.38	0.37	0.5	0.30
Atoms	5244	5122	5198	5081
Protein	5100	4978	5088	4901
Water	87	88	46	101
Magnesium	3	2	2	2
ATP	0	0	0	31
AMP-PNP	0	0	62	0
ADP	54	54	0	0
Sulfate	0	0	0	40
Sodium	0	0	0	2
Chlorine	0	0	0	4
Average *B*-factors (Å^2)[c]	66.40	79.00	28.09	70.40
Protein	66.50	79.30	28.30	70.00
Water	58.50	68.50	20.10	61.20
Ligands	65.70	72.30	20.70	107.60
PDB code	5EOY	5EOX	5EQ6	5EOU

[a] $R_{Sym} = \Sigma\Sigma|I - (I)|/\Sigma\Sigma I$, $R_{Pim} = \Sigma\sqrt{(1/(n-1)\,\Sigma|I - (I)|/\Sigma\Sigma I}$, and $CC^* = \sqrt{(2CC_{½}/(1 + CC_{½}))}$, where $CC_{½}$ is the Pearson correlation coefficient of two half-data sets, as described elsewhere (69).

[b] $R_{work} = \Sigma||F_o| - k|F_c||/|F_o|$, where F_o and F_c are the observed and calculated structure factors, respectively. R_{free} is the sum extended over a subset of reflections (5%) excluded from all stages of the refinement.

[c] As calculated using MolProbity (37).

[d] Maximum likelihood-based coordinate error, as determined by PHENIX (42).

ture as a template in Phaser (41). Through iterative rounds of building/remodeling in Coot (40) and refinement in phenix.refine (42), the structures of the SeMet-PilM·ATP, native PilM·ATP, native PilM·AMP-PNP, and native PilM·PilN(1–12)·ATP were built and refined. All structures were refined with individual B-factors except for the PilM·AMP-PNP structure, where the resolution (3.5 Å) of the data necessitated the use of grouped *B*-factors during refinement. Progress of the refinement in all cases was monitored using R_{free}.

ATPase Assays—ATPase assays were performed as described previously (43) in two independent trials done in triplicate. Briefly, in a transparent 96-well plate, 50 μl of buffer A1 (with 5 mM ATP) without imidazole was incubated with 200 μM PilM for 16 h at 37 °C. Eighty μl of 1 mM malachite green, 10% (v/v) Tween 20, and 6 mM H_2SO_4 was then added. Finally, 80 μl of 50 mM ammonium molybdate and 3.4 M H_2SO_4 was added, and the amount of phosphate released was determined by measuring absorbance at 630 nm with a SpectraMax M2 microplate reader. Comparison with a dilution series of phosphate-buffered saline permitted the quantification of the released inorganic phosphate.

Size Exclusion Chromatography Followed by Multiangle Light Scattering (SEC-MALS) Analysis—A Malvern Viscotek GPCmax system connected to a Superdex 200 Increase 10/300 GL size exclusion column (GE Healthcare) was used for SEC-MALS analysis of PilM and PilM·PilN(1–12). The column was equilibrated with buffer A2 without ATP. The intensity of light scattered by the column eluate was recorded using a Malvern 270 dual detector, and the refractive index was monitored using a VE 3580 detector. Bovine serum albumin at a concentration of 1 mg/ml was used for detector normalization. Molecular weights were calculated from Zimm plots with a protein refractive index increment (d*n*/d*c*) of 0.185 ml/g using OmniSEC version 5.10 software (Malvern Instruments Ltd.).

Bioinformatics Analysis of the N Terminus of PilM—Using BLAST (44), protein sequences with significant homology to PilM were identified. Sequences that were not annotated as a pilus or fimbrial protein, duplicate sequences, and sequences with duplicate species identifiers were removed, leaving 2231 sequences that were aligned in MEGA (45). We compared the alignment with our structure of PilM to identify sequences with N termini of greater than 7 residues, which was the size of the

motif bound by PilM. We searched these N termini for the *hXXhhX*+ motif (where *h* is a hydrophobic residue, *X* is any residue, and + is a positive residue) and the *hX*(*X*)*hh*(*X*)+ motif (where (*X*) represents an optional single residue deletion) using the SMS program (46). The motif sequences were extracted by the SMS program, and the consensus motif was visualized using WebLogo (47).

Negative Stain Electron Microscopy—EM grids (400-mesh Cu/Rh, Electron Microscopy Sciences) were overlaid with continuous carbon and subjected to glow discharge before PilM, diluted to 0.04, 0.4, or 4 μg/ml, was applied. Excess solution was blotted away after a 2-min incubation at room temperature, and the grids were rinsed three times with water. Uranyl acetate stain (0.5% (w/v)) was applied, excess stain was blotted away, and the grid was dried. Grids were examined with an FEI Technai F20 electron microscope operating at 200 kV. Images were collected with a Gatan Orius 832 CCD camera.

Bacterial Two-hybrid Analysis—Bacterial two-hybrid analysis was performed as described previously (48, 49) with the following modifications. For the plate-based assay, LB plus 20 μg/ml 5-bromo-4-chloro-3-indolyl-β-D-galactopyranoside or MacConkey plates with 1% (w/v) maltose and 0.5 mM isopropyl-D-1-thiogalactopyranoside were spot-inoculated with 0.5 μl of *E. coli* previously grown to an A_{600} of 0.5. Plates were read after 64 h. For the quantitative assay, 500 μl of *E. coli* grown at 30 °C to A_{600} were pelleted at 2300 × *g*. The pellet was resuspended in 50 μl of 200 mM Na_2HPO_4, pH 7.4, 20 mM KCl, 2 mM $MgSO_4$, 0.8 mg/ml cetyltrimethylammonium bromide detergent, 0.4 mg/ml sodium deoxycholate, and 0.54% (v/v) β-mercaptoethanol. 150 μl of a second solution was then added: 60 mM Na_2HPO_4, pH 7.4, 40 mM KCl, 1 mM *ortho*-nitrophenyl-β-galactoside, 20 μg/ml cetyltrimethylammonium bromide, 10 μg/ml sodium deoxycholate, and 0.27% (v/v) β-mercaptoethanol. The A_{420} and A_{550} were measured every 5 min for 1 h at 30 °C in a plate reader. β-Galactosidase activity was calculated by finding the slope of $(A_{420} - 1.75 \times A_{550})/(0.5 \times$ absorbance units $\times$ 0.5 ml) over time (min) relative to a positive control (pKT25::zip with pUT18C::zip). PilN, PilM, and PilO pKT25 and pUT18C constructs were described previously (50). PilU constructs were cloned with primers PilU_F and PilU_R. PilT constructs were cloned with primers PilT_F and PilT_R. PilM·PilN(1–12) constructs were cloned with primers PilMN1–12_F and PilMN1–12_R. PilA constructs were cloned with primers PilA_F and PilA_R. PilC constructs were cloned with primers PilC_F and PilC_R. PilB constructs were cloned with primers PilB_F and PilB_R. Cloning and subcloning was accomplished by XbaI, EcoRI, and KpnI digestion where appropriate, followed by ligation. The fidelity of the sequences was verified by TCAG sequencing facilities (Hospital for Sick Children).

Biolayer Interferometry—PilM and PilN(1–12) binding kinetics were determined by biolayer interferometry using an Octet RED96 (ForteBio). All binding reactions were performed at 25 °C in buffer B3 without imidazole with 0.2% (v/v) Triton X-100, 0.01% (w/v) bovine serum albumin, and 2 mM ATP or ADP. Streptavidin biosensors were loaded with 1 μM synthetic PilN(1–12) C-terminally linked to lysine-biotin by PEG6 (GenScript), quenched with 10 μg/ml biocytin, and then exposed to varying concentrations (1–100 μM) of PilM. The signal from reference wells without PilN(1–12) conjugated to the biosensors or from which PilM had been omitted were subtracted from all binding curves before curve-fitting analysis was performed using ForteBio Data Analysis version 8.1.

In Vitro Pull-down Experiments—For pull-downs, 100 μM PilM or PilM·PilN(1–12) was incubated with 100 μM PilB or PilT in 50 μl of buffer B3 for 1 h at 20 °C. As described above, the PilM constructs were treated with thrombin, and the His tag was removed while both PilB and PilT were His-tagged. The proteins were then applied to 50 μl of pre-equilibrated Ni-NTA-agarose resin, washed with 35 ml of buffer B3 plus 10 mM arginine, and eluted in 50 μl of buffer B3 plus 300 mM imidazole. Eight microliters were then separated on SDS-PAGE, and Western blot analysis was performed using rabbit anti-PilM (16), anti-PilB (10), and anti-PilT (17) antibodies. Goat anti-rabbit HRP conjugate (Bio-Rad) was used to detect PilM, PilT, or PilB by chemiluminescence (Thermo Fisher Scientific).

Isothermal Titration Calorimetry of PilM with ATP and ADP—The dissociation constant (K_d) for nucleotide binding was determined using isothermal titration calorimetry (ITC) using a MicroCal Auto-iTC200 (Malvern Instruments Ltd.) at 10 °C. PilM was used directly from the SEC column without further concentration to avoid buffer mismatch. 200 μl of 96 μM PilM, 73 μM PilM·PilN(1–12), 77 μM PilM K52A, or 55 μM PilM S19A were injected into the cell. 2 μl of SEC buffer or 1.5 mM ATP or 1.5 mM ADP resuspended in the SEC buffer were injected into the cell containing PilM. A total of 25 injections were performed with an equilibration time of 150 s between injections. The data were fitted with Origin 7 ITC analysis software using a single-site binding model.

Results

Improving the Solubility of P. aeruginosa PilM—Initial *E. coli* expression and purification of *P. aeruginosa* PilM revealed that the protein was poorly expressed, found predominantly in high molecular weight aggregates, and that it precipitated rapidly following purification. The crystallizability of *T. thermophilus* PilM ($PilM_{Tt}$) was improved by incubating it with a peptide corresponding to the cytoplasmic N-terminal portion (residues 1–15) of $PilN_{Tt}$, although only residues 1–8 were identified in the resulting electron density (15). Similarly, in the crystal structure of cytoplasmic GspL, residues 1–12 of its PilN-like portion could be modeled (51). In an attempt to improve the solubility of *P. aeruginosa* PilM, we fused the cytoplasmic portion of PilN (residues 1–12) via a 3-residue linker to the C terminus of PilM (PilM·PilN(1–12)). Although PilM·PilN(1–12) also precipitated after purification, we exploited this property in a solubility screen to find a more compatible purification buffer. The solubility of PilM·PilN(1–12) was improved in 50 mM Tris and 30 mM citrate, pH 6.0, 150 mM NaCl, 10% (v/v) glycerol, 2 mM tris(2-carboxyethyl)phosphine, 5 mM $MgCl_2$, and 5 mM ATP. Conveniently, this buffer also improved solubility and reduced aggregation of native PilM.

Structure Determination of PilM and PilM·PilN(1–12)—To study potential structural changes upon PilM-PilN interaction, we determined the crystal structures of PilM and PilM·PilN(1–

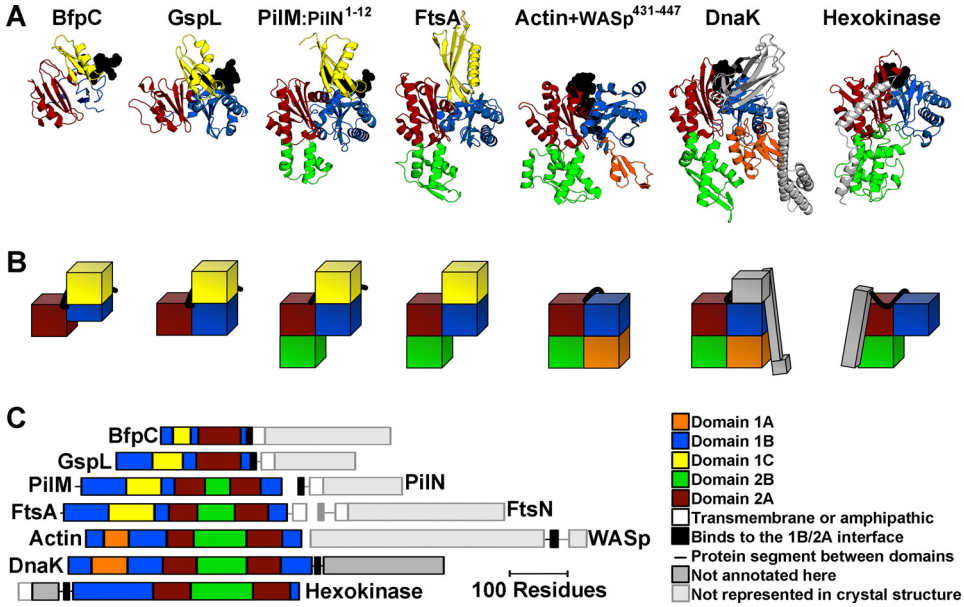

FIGURE 2. **Structural comparison of PilM with homologs.** *A*, PilM homologs were aligned to PilM·PilN(1–12) using SPalign-NS (68). From *left* to *right*, BfpC from *E. coli* (PDB code 3VHJ, $RMSD_{C\alpha}$ = 2.2 Å over 106 residues); GspL from *Vibrio cholerae* (PDB code 2BH1, $RMSD^{C\alpha}$ = 2.0 Å over 159 residues); FtsA from *Thermotoga maritima* (PDB code 4A2A, $RMSD_{C\alpha}$ = 1.9 Å over 257 residues); actin α1 from *Oryctolagus cuniculus* (PDB code 2A3Z, $RMSD_{C\alpha}$ = 2.0 Å over 192 residues); DnaK from *E. coli* (PDB code 4B9Q, $RMSD_{C\alpha}$ = 2.1 Å over 216 residues); and hexokinase-1 from *Schistosoma mansoni* (PDB code 1BDG, $RMSD_{C\alpha}$ = 2.4 Å over 196 residues). The individual domains are *color-coded* according to actin and FtsA domain definitions (29, 30): *yellow*, 1C domain; *blue*, 1B domain; *red*, 2A domain; *green*, 2B domain; *orange*, 1A domain; *gray*, not annotated here; *faded gray*, not in the crystal structure. Protein segments that lie across the 1B/2B interface are represented as *black spheres*. *B*, the domain architecture is also represented in *schematic blocks* and *color-coded* as in *A*. *C*, the linear domain architecture for each protein is represented to scale.

12). PilM and PilM·PilN(1–12) crystallized in a number of different conditions. Those that favored the growth of large single crystals of PilM and PilM·PilN(1–12) were identified after optimization (Table 2). The crystals of PilM and PilM·PilN(1–12) indexed to space groups $P2_12_12$ and $P321$, respectively, and diffracted to 2.4 Å. Because we were unable to solve the structure of PilM or PilM·PilN(1–12) by molecular replacement using the available structure of $PilM_{Tt}$·$PilN_{Tt}$(1–15), a SeMet derivative of PilM was crystallized, and its structure was determined using the single wavelength anomalous diffraction technique to 2.5 Å resolution. The structures of native PilM and PilM·PilN(1–12) were subsequently solved by molecular replacement using our SeMet-PilM structure as a template, and both were found to have two PilM molecules in the asymmetric unit. Model building and refinement produced final structures of SeMet-PilM, PilM, and PilM·PilN(1–12) with R_{work}/R_{free} values of 20.7/26.2, 22.4/25.7, and 21.1/23.8%, respectively. Some residues could not be modeled due to poor electron density. The entire PilM sequence could be modeled into both molecules in the asymmetric unit of the SeMet PilM structure, except for residue 9 of one molecule. In both molecules of the asymmetric unit in the native PilM structure, the entire PilM sequence could be modeled, except for residues 8 and 9. In one molecule of the PilM·PilN(1–12) structure, residues 9–99, 116–128, 132–241, 244–354, and 359–367 were modeled, and in the other molecule, residues 10–132, 134–186, 189–355, and 358–366 were modeled.

The PilN Binding Pocket of PilM Is Highly Conserved—As previously reported for the structure of $PilM_{Tt}$·$PilN_{Tt}$(1–15) (15, 24, 28), our PilM structures were similar to those of FtsA, GspL, and BfpC (Fig. 2) as well as to Hsp70 family chaperones such as DnaK, eukaryotic and bacterial actins such as actin α1, and sugar kinases like hexokinase 1. Aligning the structures of PilM with FtsA, GspL, BfpC, DnaK, actin α1, and hexokinase 1 not only illustrates the diversity of domains found in the actin/Hsp70/hexokinase superfamily but also reveals that domains 2A and 1B are present in each actin/Hsp70/hexokinase superfamily member identified herein, with domain 2A inserted within domain 1B.

The 1B and 2A domains also create an interface that binds inter- or intramolecular peptides in all superfamily members identified herein. For PilM, this peptide is the cytoplasmic N terminus of PilN. For GspL and BfpC, this peptide corresponds to the cytoplasmic PilN-like portion of GspL or BfpC, respectively. For FtsA, this peptide is expected to correspond to the N terminus of FtsN (32, 34), as mentioned above, although as yet there are no corroborating structural data. This peptide in DnaK corresponds to the linker region between the actin-like portion of DnaK and its substrate-binding domain. For hexokinase, this peptide corresponds to the linker region between an N-terminal domain and the actin-like portion of hexokinase. For actin, this peptide corresponds to the WH2 motif of Dnase I, and several other peptides bind actin at this same interface (53). Peptide binding at this interface is thus a conserved feature of PilM paralogs.

Comparison of our *P. aeruginosa* PilM·PilN(1–12) structure with that of $PilM_{Tt}$·$PilN_{Tt}$(1–15) (15) revealed that the mode of binding of PilM to PilN was highly conserved and amphipathic (Fig. 3*A*). In both species, PilN Ile-4 (Leu-4 in *T. thermophilus*), Leu-6, and Leu-7 are tucked into hydrophobic pockets; Asn-5 forms hydrogen bonds with the backbone of residues Lys-166 (Val-168) and Val-168 (Leu-170); and Arg-3 forms a salt bridge

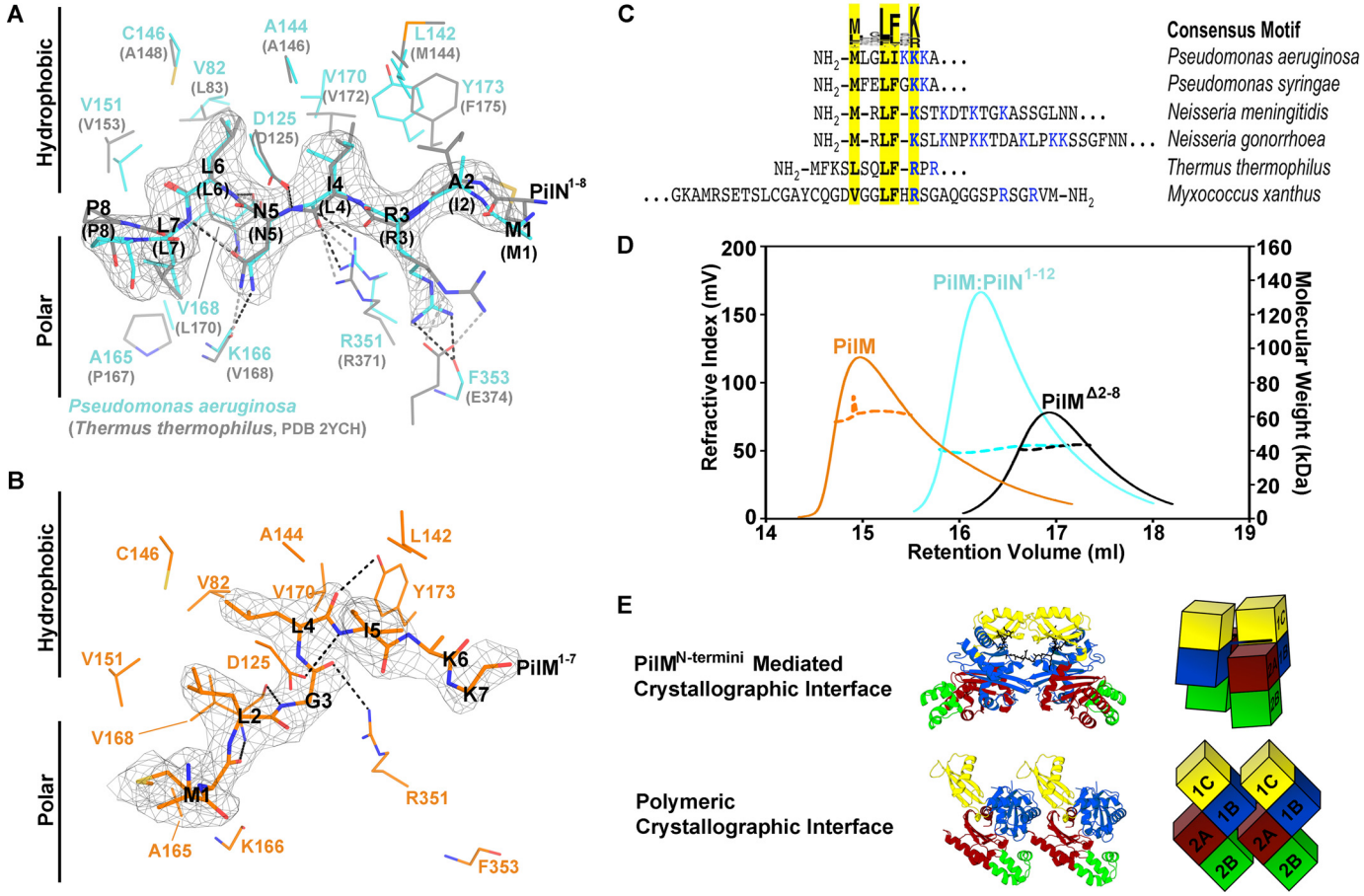

FIGURE 3. **The PilN binding pocket of PilM.** *A*, the PilN peptide in the PilN binding pocket of PilM·PilN(1–12) from *P. aeruginosa* (*cyan*) was aligned with $PilM_{Tt}$·$PilN_{Tt}$(1–15) (*gray*; PDB code 2YCH; $RMSD_{C\alpha}$ = 1.9 Å over 266 residues), and residues in the respective PilM binding pockets are shown. The *gray mesh* represents the $2|F_o| - |F_c|$ omit electron density for *P. aeruginosa* PilM·PilN(1–12) calculated without PilN and contoured at 1σ. *B*, N terminus of PilM bound in the PilN binding pocket. The *gray mesh* represents the $2|F_o| - |F_c|$ omit electron density map calculated without residues 1–9 and contoured at 1σ. Residues important for PilM(1–7) binding are shown. *C*, alignment of selected PilM N termini from model organisms showing the MXXLFXK consensus motif. *D*, size exclusion chromatography (*solid line*) and multiangle light scattering (*horizontal dashed line*) analysis of PilM (*orange*), PilM·PilN(1–12) (*cyan*), and $PilM^{\Delta 2-8}$ (*black*). *E*, PilM interfaces identified in the PilM crystal structure represented in *schematic blocks* with the individual domains of PilM *color-coded*: *yellow*, 1C domain; *blue*, 1B domain; *red*, 2A domain; *green*, 2B domain.

with a residue near the C terminus. In *T. thermophilus*, Arg-3 forms a salt bridge with Glu-374 in PilM, whereas in *P. aeruginosa*, Arg-3 forms a salt bridge with the backbone of Phe-353 in PilM. The PilM-PilN interface buries 610 Å^2 with a binding free energy of −4.9 kcal/mol, as calculated by PDBePISA (52).

The PilN Binding Pocket of PilM Is Promiscuous—Although the *P. aeruginosa* PilM·PilN(1–12) and $PilM_{Tt}$·$PilN_{Tt}$(1–15) structures are remarkably similar ($RMSD_{C\alpha}$ = 1.9 Å), our PilM structure, the first to be determined without a PilN peptide bound, exhibits a number of novel features. Examination of the PilM structure revealed that its PilN binding pocket was occupied. We found continuous electron density from the PilN binding groove to the N terminus of the second PilM protomer in the asymmetric unit and were able to build the 7 N-terminal residues of PilM (PilM(1–7)) into this density (Fig. 3*B*). As detailed above, these residues could not be modeled in the PilM·PilN(1–12) structure. Examination of this interaction revealed that PilM(1–7) was oriented antiparallel to the PilN peptide in the PilM·PilN(1–12) structure, with residues Met-1, Leu-4, and Ile-5 of PilM playing roles similar to Leu-7, Leu-6, and Ile-4 of PilN in PilM·PilN(1–12), respectively. Although the side chain of PilM Lys-7 could not be modeled, the position of the main chain atoms is similar to that of PilN Arg-3.

PilM(1–7) adopts a bent configuration compared with the extended conformation of PilN. The bend originates between PilM Leu-4 and Ile-5. PilM Leu-4 and Ile-5 appear to stretch to occupy the sites occupied by PilN Leu-6 and Ile-4 in PilM·PilN(1–12). PilN Leu-6 and Ile-4 do not need to stretch because Asn-5 separates them, and thus PilN remains extended. The bent configuration of PilM(1–7) appears to hold the PilN binding pocket open. Despite these differences, the buried surface area (620 Å^2) and binding free energy (−8.8 kcal/mol) of the PilM(1–7) interaction are similar to values calculated for the PilM-PilN peptide interaction.

The N Terminus of PilM Contains a Conserved Motif Necessary for PilM Dimerization—Structural comparison of PilM·PilM(1–7) binding with PilM·PilN(1–12) binding indicated that the N-terminal residues Met-1, Leu-4, Ile-5, and Lys-7 play a key role in the binding of the N-terminal peptide to the protein. If the binding of PilM(1–7) had functional implications, we hypothesized that a similar pattern of residues should be found in other PilM orthologues. PilM orthologues from

unique species were aligned to our structure of PilM to define the flexible N terminus from the globular portion of PilM. This analysis revealed that approximately two-thirds of PilM orthologues have at least an extra 7 flexible N-terminal residues. Due to variations in length and sequence, these PilM N termini align poorly. Despite this, 54% of N termini have an *hXXhhX*+ motif. Allowing optional single residue deletions, denoted by (*X*) in *h*X(*X*)*hh*(*X*)+, allows this motif to be found in 80% of the sequences examined. Although our motif search was for any hydrophobic or positive residues in the *h*XX*hh*X+ pattern, there was a clear sequence preference for an MXXLFXK motif, which closely matches the sequence of *P. aeruginosa* PilM(1–7). Following the MXXLFXK motifs are usually positive residues interspersed with polar residues. Using this information, we identified potential motifs in the N termini of PilM proteins from well studied model systems (Fig. 3*C*).

SEC-MALS of PilM and PilM·PilN(1–12) indicated that there were quaternary structural changes in PilM upon binding PilN. In solution, the data suggest that PilM was a mixture of monomer and dimer (59 kDa), whereas PilM·PilN(1–12) was monomeric (41 kDa) (Fig. 3*D*). We therefore examined the crystal contacts in the PilM structure for potential dimeric interfaces. There were two potential interfaces: the interface created by the binding of PilM(1–7) by the PilM protomers in the asymmetric unit (buried surface area and binding free energy of 1580 Å^2 and −17.8 kcal/mol, respectively) and a polymeric interface (buried surface area and binding free energy of 720 Å^2 and −6.6 kcal/mol, respectively) (Fig. 3*E*). The latter interface is similar (albeit offset by a ~4-nm translation) to the "actin-like" interface through which FtsA polymerizes (29, 30); both of these PilM and FtsA interfaces involve head-to-tail interactions between similar domains. Because typical protein-protein interactions have buried surface areas of >600 Å (54), either of the N-terminal or FtsA-like interfaces might be responsible for the dimerization of PilM.

Similar to FtsA, the actin-like interface of PilM suggested that it could potentially form higher order oligomers. However, negative stain EM revealed no PilM oligomers. To further explore the dimer interface, we deleted the first 8 N-terminal residues of our PilM construct (PilM$^{\Delta 2-8}$). SEC-MALS analysis showed that PilM$^{\Delta 2-8}$ was monomeric in solution (Fig. 3*D*), indicating that the N terminus of PilM was important for homodimer formation. These data are consistent with PilM (1–7) binding to the PilN binding pocket in the crystallographic dimer. These data are also consistent with the monomeric structure of PilM·PilN(1–12) because the binding of PilN to PilM would prevent the PilM self-interaction.

Lys-52 and Ser-19 Are Important for but Not Essential to ATP Binding—Examination of the electron density map revealed the presence of nucleotide in both the PilM and PilM·PilN(1–12) structures. Although we added ATP to our crystallization buffer, we found that modeling ADP and magnesium best fit the electron density observed in the PilM structure (Fig. 4*A*). This suggests that either the terminal phosphate was disordered or that ATP was hydrolyzed during the crystallization process. If the latter is the case, hydrolysis was likely to be non-enzymatic, because we and others (15) have been unable to demonstrate *in vitro* ATPase activity for either PilM or PilM·PilN(1–12). However, aligning the ATP-binding site of PilM with homologous ATPase DnaK (PDB code 4B9Q) revealed a high degree of conservation in the residues necessary for ATP catalysis, including Lys-52 and Glu-171 of PilM, which align with the catalytic residues Lys-70 and Glu-171 of DnaK (55) (Fig. 4*B*). In the PilM structure, Lys-52 and Glu-171 are shifted away from the γ-phosphate of ATP by 3 Å compared with corresponding Glu-171 and Lys-70 of DnaK. Thus, PilM could potentially have ATPase activity if a conformational change brought Lys-52 and Glu-171 closer to the γ-phosphate.

To model the γ-phosphate, we crystallized PilM in the presence of AMP-PNP (Fig. 4*C*). These crystals diffracted to lower resolution (3.5 Å), but valuable information could still be derived. Residue Lys-52 was disordered in the PilM·ADP structure but ordered in PilM·AMP-PNP structure. Lys-52 and Ser-19 appear to facilitate coordination of the γ-phosphate of ATP. To confirm that these residues participate in ATP binding, we made S19A and K52A PilM variants and evaluated their ATP-binding affinity using ITC (Fig. 4*E*). The binding of ATP to PilM was enthalpy-driven, with a K_d of 4.63 ± 0.05 μM, whereas binding of ADP to PilM was too weak to be quantified. Compared with wild type, the PilM^{S19A} and PilM^{K52A} variants have ~6- and 4-fold reduced affinity for ATP, respectively. These data suggest that Ser-19 and Lys-52 are each important but not essential for ATP binding.

Examination of the active sites of the two protomers in the asymmetric unit of the PilM·PilN(1–12) structure revealed electron density that could be best fit as ATP and magnesium in one protomer (Fig. 4*D*). In the second protomer, sulfate, which was present in the crystallization buffer, appeared to be bound in the ATP-binding pocket. As in the PilM·AMP-PNP structure, Ser-19 and Lys-52 coordinated the γ-phosphate of ATP. The binding affinity of PilM·PilN(1–12) for ATP was similar to that of PilM (4.37 ± 0.05 μM) (Fig. 4*E*).

PilN Binding Causes Tertiary Structure Changes in PilM—Comparing the overall structures of PilM bound to ADP *versus* AMP-PNP revealed a ~5° rotation of domain 1B with respect to domain 2A (Fig. 5*A* and supplemental Animation 1). Comparison of the AMP-PNP-bound structure of PilM with the ATP-bound structure of PilM·PilN(1–12) revealed a conformational change in PilM upon binding PilN (Fig. 5*B* and supplemental Animation 2). Using DynDom (56), we determined that Domain 1C of PilM undergoes a hinge-bending motion of ~25° that clamps the PilN peptide between the 1C and 1B domains. In a corresponding lever-like motion, a loop in the 1C domain of PilM (residues 83–85, loop 1B) moves 7 Å, whereas domain 1B rotates ~10° with respect to domain 2A. These motions bring the loop containing Lys-52 closer to ATP by 2 Å.

Because binding of AMP-PNP to PilM *versus* PilN to PilM rotated domain 1B in opposing directions, we hypothesized that ATP binding could modulate PilN binding. We tested this hypothesis using biolayer interferometry with a biotinylated peptide of PilN(1–12) attached to the biosensor (Fig. 5*C*). The K_d, k_{on}, and k_{off} values of PilM for PilN(1–12) with 2 mM ATP were 3.27 ± 0.03 μM, 20,800 ± 200 M^{-1} s^{-1}, and 67,900 ± 200 s^{-1}, respectively. The dissociation constant of PilM corresponds to a half-life of ~10 s. The affinity of PilM for PilN(1–12) was 2-fold higher in the presence of ATP than ADP. The

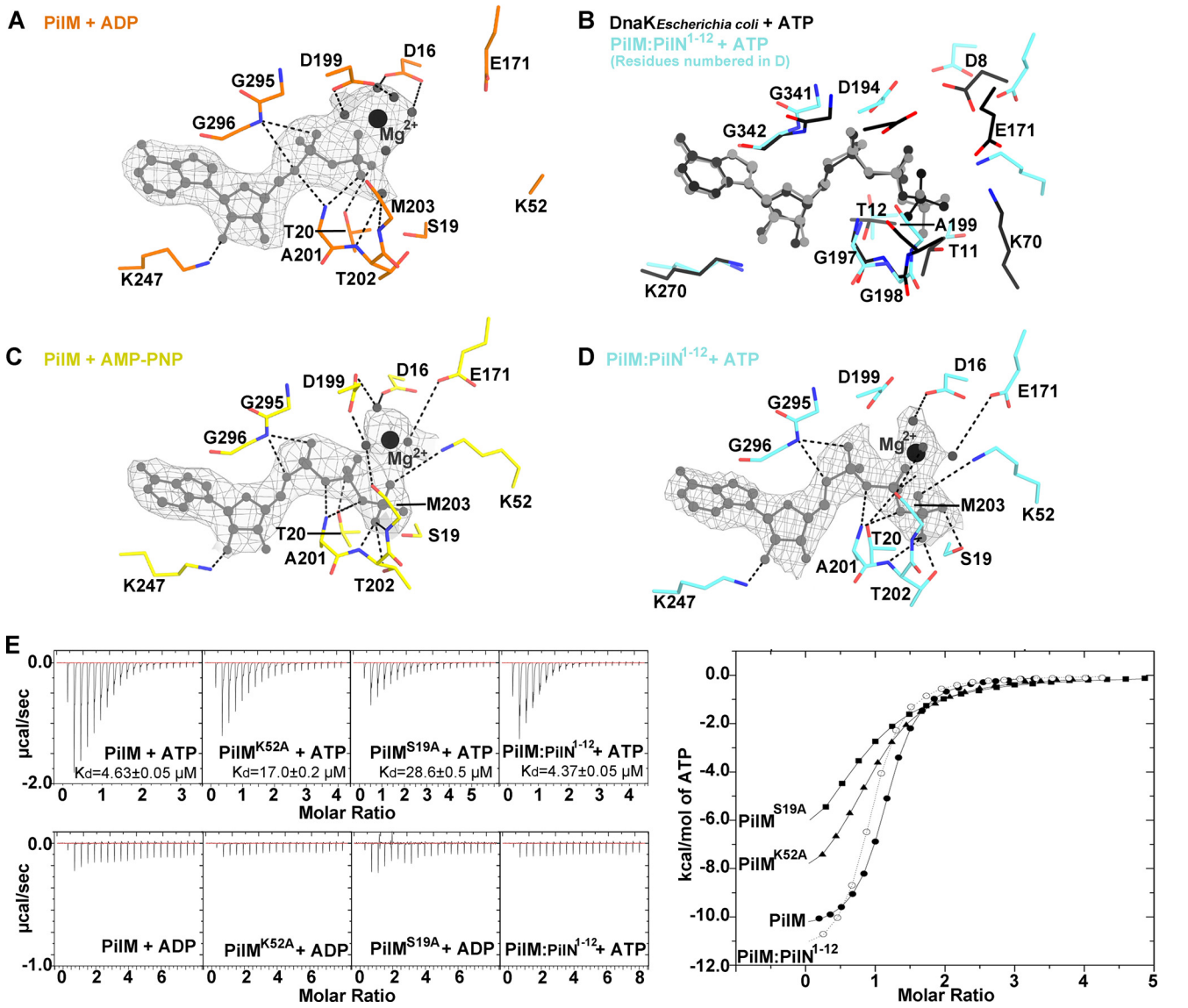

FIGURE 4. **Structural analysis of ATP binding to PilM.** Shown are *stick representations* of the ATP binding site of the PilM·ATP (*A*), PilM·AMP-PNP (*B*), and PilM·PilN(1–12)·ATP (*C*) structures. Direct polar contacts are shown as *dashed lines*. ADP, ATP, and AMP-PNP are shown in *light gray*, waters coordinated by magnesium are shown as *small dark gray spheres*, and magnesium is shown as a *large black sphere*. The *gray mesh* represents the $2|F_o| - |F_c|$ omit electron density calculated without nucleotide and contoured at 1σ. *D*, DnaK (*black*) from *E. coli* (PDB code 2B9Q) bound to ATP aligned with PilM·PilN(1–12)·ATP (*cyan*). Structures were aligned by superimposing the ATP ligand. *E*, isothermal titration calorimetry analysis of PilM, PilM^{K52A}, PilM^{S19A}, and PilM·PilN(1–12) titrated with ATP or ADP. The raw data of each PilM construct are plotted in μcal/s on the *left* with the calculated dissociation constant (K_d) indicated. The integrated data for each ATP titration are plotted on the *right*; PilM is plotted as a *filled circle*, PilM^{S19A} as a *filled square*, PilM^{K52A} as a *filled triangle*, and PilM·PilN(1–12) as an *empty circle*.

dissociation rate was the same regardless of which nucleotide was present. We also evaluated the binding of the PilM^{K52A} and PilM^{S19A} variants to PilN. Like wild-type PilM, the affinity of PilM^{S19A} for PilN(1–12) was 2-fold higher in the presence of ATP than ADP. Conversely, the affinity of PilM^{K52A} for PilN(1–12) was the same with ADP or ATP. These data suggest that ATP binding increases the association of PilM and PilN(1–12) and that Lys-52 is necessary for ATP to mediate this effect.

PilM Bridges PilN, PilB, PilT, and PilC—Based on data from the homologous T2S and T4bP systems, we hypothesized that in addition to ATP and PilN, PilM will bind to additional components of the T4aP system. BACTH assays (57) have been used previously to analyze the connectivity of cytoplasmic T4aP proteins in *Neisseria meningitidis.* These data suggested interactions between PilM and PilT2, a PilT paralog not present in *P. aeruginosa* (58). To determine whether additional binding partners could be identified in *P. aeruginosa* with our PilM constructs, we performed BACTH analysis with both PilM and PilM·PilN(1–12) using two assay outputs, MacConkey-maltose and the β-galactosidase assay.

Although the interactions observed for the cytoplasmic proteins in *P. aeruginosa* are similar to those reported for *N. meningitidis*, there are several important differences (Fig. 6, *A* and *B*). As were seen in *N. meningitidis*, using the MacConkey-maltose assay, we identified interactions between PilC and PilA, PilC and PilO, PilC and PilT, PilT and PilU, PilT and PilB, PilM and PilN, PilN and PilO, and PilO and PilA as well as PilA/B/C/M/O/T/U self-interactions. We also observed an PilC-PilU

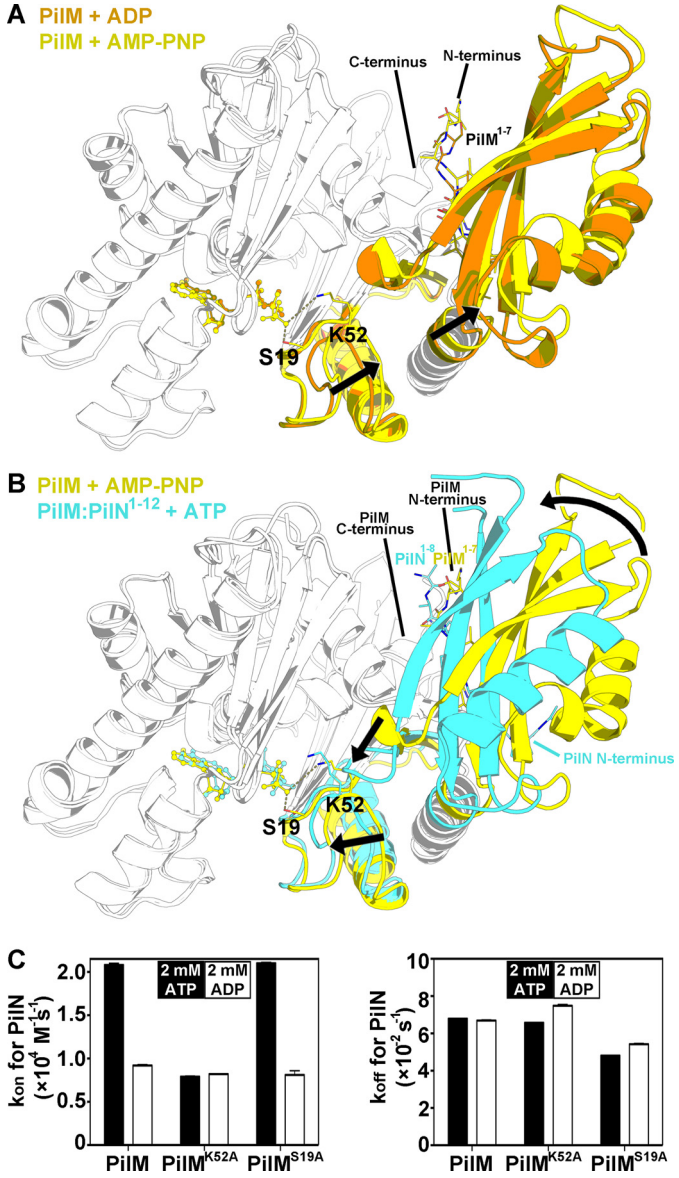

FIGURE 5. **Tertiary structure changes in PilM upon ATP or PilN binding.** Alignment of the structures of PilM·ADP (*orange*), PilM·AMP-PNP (*yellow*), and PilM·PilN(1–12)·ATP (*cyan*) is shown. Structures were aligned by pairwise alignment of the 2A and 2B domains (residues 185–318). Ser-19 and Lys-52 are represented by *stick representations* in the ATP and AMP-PNP complexed structures. For clarity, regions of the structure that do not undergo large structural changes have been *colored white*. The N and C termini have been *labeled*. The N terminus of PilM is located at the *back* of the image and thus not labeled; the labeled PilM N terminus represents the N terminus of PilM from the adjacent protomer in the asymmetric unit. *A*, alignment of PilM bound to ADP and AMP-PNP. *B*, alignment of PilM bound to AMP-PNP and PilM·PilN(1–12) bound to ATP. *C*, the binding kinetics of PilM for Biotin·PilN(1–12) were determined by biolayer interferometry in the presence of 2 mM ATP (*black bars*) or 2 mM ADP (*open bars*). Data represent the mean of four PilM dilutions, and the *error bars* represent the S.E.

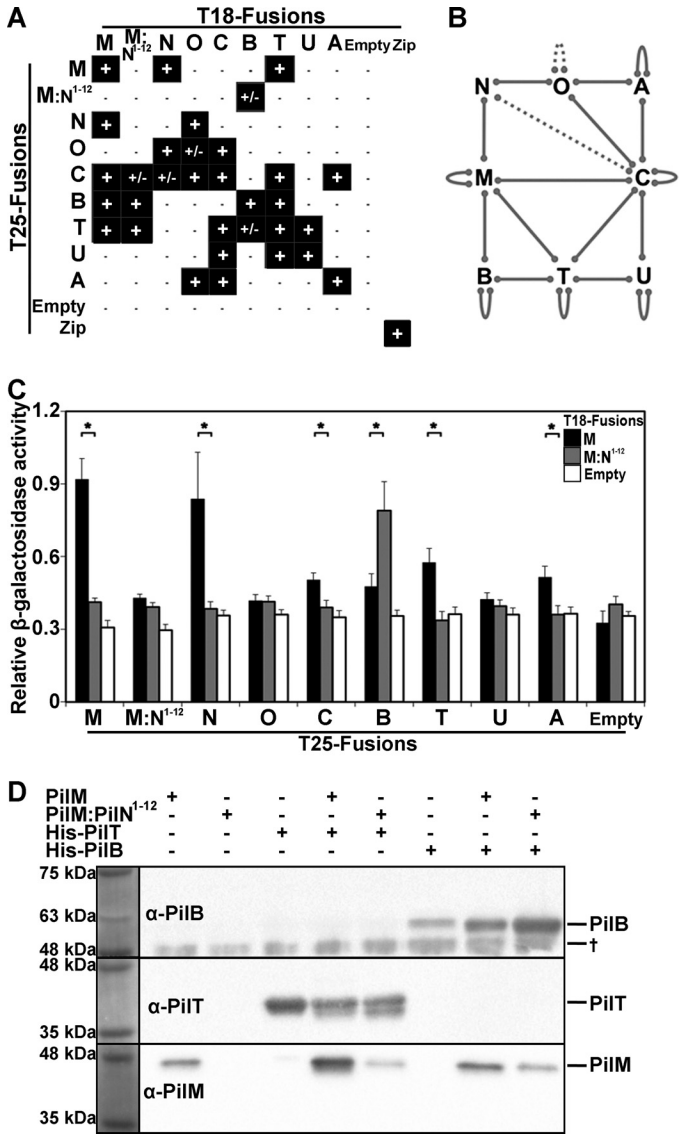

FIGURE 6. **Identification and comparison of PilM and PilM·PilN(1–12) interactions with PilB, PilT, and PilC.** *A*, qualitative BACTH results from MacConkey-maltose agar assay. Colonies that turned red are indicated with a *plus sign* to denote an interaction; colonies that remained white are indicated with a *minus sign* to denote no interaction; and colonies that displayed an intermediate phenotype (speckled or inconsistently red colonies) are indicated with a *plus/minus sign*. *B*, *P. aeruginosa* BACTH results represented as *solid lines* for positive (+) results and *dotted lines* for intermediate (+/−) results. *C*, quantitative BACTH β-galactosidase assay results. pKT25 with a PilM-M::N$^{1-12}$/N/O/C/B/T/U/A insert was co-transformed with pUT18C:PilM (*black*), pUT18C:PilM·PilN(1–12) (*gray*), or empty pUT18C (*white*). Data represent the mean, and the *error bars* represent the S.E. The assay was performed in eight replicates. *, $p < 0.05$, Student's *t* test. *D*, *in vitro* PilM and PilM·PilN(1–12) pull-down experiments with His-tagged PilB and PilT. The His-tagged proteins were pulled down using nickel affinity chromatography and visualized by Western blot analysis as indicated. Two PilT bands are evident and may represent partial breakdown. †, a band non-specifically bound by the PilB antibody.

interaction and PilM-PilB, -PilT, and -PilC interactions. It is not clear whether these additional interactions are absent in the *N. meningitidis* T4aP system or if *P. aeruginosa* proteins are more amenable to BACTH analysis. Interactions between PilM-PilC and PilM-PilB equivalents in the T2S system have been described previously (24, 27). Consistent with our SEC-MALS data, we detected PilM self-interactions but not PilM·PilN(1–12) self-interactions. Our BACTH analysis broadens our understanding of the connectivity of the cytoplasmic T4aP components and highlights the central position of PilM.

Comparing the BACTH signals using the β-galactosidase assay suggests that whereas PilM and PilM·PilN(1–12) bind PilB, PilT, and PilC, their affinities for these proteins are different (Fig. 6*C*). Specifically, PilM·PilN(1–12) interacts preferen-

tially with PilB, and PilM interacts preferentially with PilC and PilT. The β-galactosidase assay also suggested an interaction between PilA and PilM, which was not identified using the MacConkey-maltose assay, underscoring the necessity for secondary validation of interactions identified by BACTH.

Validating these differential interactions *in vitro* has not been possible. Purified PilB and PilT each have ATPase activity, suggesting that they are folded properly, but PilM and PilT aggregated in our biophysical instruments, impeding analysis. However, we could validate a direct interaction between PilM and PilB or PilT using *in vitro* co-purification studies. Whereas PilM showed some nonspecific binding to the Ni-NTA resin, additional PilM was co-purified with His-tagged PilB or PilT (Fig. 6*D*). PilM·PilN(1–12) did not nonspecifically bind to the Ni-NTA resin and more clearly co-purified with His-tagged PilB and PilT, providing evidence that PilM interacts directly with PilB and PilT *in vitro*.

Discussion

In this study, we characterized two distinct PilM conformations using crystallographic, biophysical, biochemical, and BACTH analyses. We identified conserved peptide motifs that bind to each of these conformations, supporting the relevance of both. Further, we have extended the PilM protein interaction network and demonstrated using two different methods that PilM binds to PilB and PilT.

An intriguing feature of our PilM crystal structure is the interaction we observed between PilM(1–7) and the adjacent PilM protomer. This peptide occupies the PilN binding groove and facilitates the formation of a PilM homodimer. Although we have not determined whether PilM homodimerizes *in vivo*, comparison with other species revealed that the residues involved in this interaction are a conserved feature of PilM. PilM(1–7) and PilN(1–8) residues make similar contacts in the binding pocket, and both are followed by positive residues interspersed with polar residues. The N terminus of FtsN bound by the PilM homolog FtsA also has a conserved motif followed by interspersed positive residues (32) extending the number of conserved features between PilN and FtsN. PilN(1–8) and PilM(1–7) have amphipathic characteristics, reflecting the nature of the PilN binding pocket of PilM. These amphipathic qualities and membrane proximity suggest that PilN(1–8) and PilM(1–7) could be membrane-associated when not bound to PilM. The PilM homologues, FtsA and MreB, have membrane-associated C- and N-terminal amphipathic helices, respectively (59, 60). The amphipathic C-terminal helix of FtsA maintains FtsA in a non-polymerized conformation until FtsA is adjacent to a lipid bilayer (61). Thus, PilM(1–7) might keep PilM in a dormant conformation until PilN binding, or it may keep PilM stable when temporarily disengaged from PilN.

The structural analysis in this study revealed that peptide binding at an interface created by domains 1B and 2A is highly conserved in actin/Hsp70/hexokinase superfamily proteins. This interface corresponds to the PilN binding pocket of PilM and may be a conserved binding site because it is located at a hinge point that can rotate upon ATP binding (62). Hence, where it has been evaluated, peptide binding to this interface can be modulated by ATP binding and/or catalysis (53, 63).

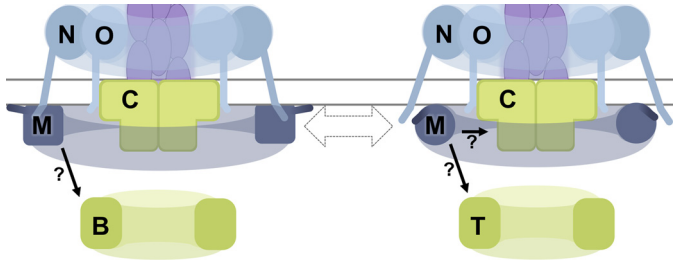

FIGURE 7. **Working model with PilM binding and dissociating from PilN modulating the binding partners of PilM.** PilM adopts different conformations when it is bound to itself (via PilM(1–7), shown as a *darker line* connected to PilM) or PilN (the N terminus of which is depicted in the cytoplasm). The identification of a conserved motif in PilM(1–7) bound by PilM as well as transient binding kinetics suggest that PilM is not always bound to PilN. In addition to PilN, PilM binds PilB, PilT, and PilC, and BACTH results suggest that these binding events could be modulated by the PilN-dependent conformation of PilM.

This is consistent with our finding that ATP binding to PilM increased PilN affinity ~2 fold. In DnaK, ATP binding increases affinity for the interdomain linker peptide, ^{389}VLLL^{392} (63). When DnaK binds the ^{389}VLLL^{392} peptide, a substrate peptide bound to a different interface is released (63). Hence, substrate release is dependent on ^{389}VLLL^{392} binding, which is itself dependent on ATP binding. Mutating Lys-70 in DnaK prevents ATP-dependent release of substrate peptide (64). Thus, it seems likely that Lys-70 in DnaK enables ATP to increase the affinity of DnaK for the ^{389}VLLL^{392} peptide. PilM Lys-52 aligned structurally with DnaK Lys-70, and mutation of PilM Lys-52 similarly nullified the ATP-mediated increase in PilN binding. Lack of the 2B domain necessary to bind ATP in GspL and BfpC of the T2S and T4bP systems (28) suggests that GspL and BfpC do not need to regulate association to their PilN-like portions, consistent with fusion of these domains.

We found that the half-life of the PilM-PilN(1–12) interaction is ~10 s, suggesting that PilN may disengage from PilM on a time scale of relevance to type IV pilus dynamics. For example, the pilus of *P. aeruginosa* is expected to extend or retract for ~1–14 s, because pili lengths vary from 1 to 7 μm, and the mean extension and retraction rate is 0.5 ± 0.2 μm/s (65, 66). In other words, the PilM-PilN interaction may be just long enough for a cycle of extension or retraction and thus could have functional implications for these or related processes.

At the time of manuscript submission, these analysis provided the first evidence for any T4aP system that PilM directly interacts with PilB and PilT and provided BACTH data to suggest that PilM might bind PilC. Before manuscript publication, it was demonstrated that PilM directly interacts with PilB in *Myxococcus xanthus* (67), corroborating our results. Both BfpE, the PilC homologue in the T4bP system, and GspE, the PilB homologue in the T2SS, have been shown to bind to the PilM loop 1B equivalents in BfpC and GspL, respectively (24, 51). We predict that PilM interacts with PilB and potentially PilC using a similar interface. Comparing the structures of PilM and PilM·PilN(1–12) revealed that residues in loop 1B move by 7 Å in the presence of the PilN peptide. Likewise, our BACTH data suggested that interaction of PilM with PilN differentially impacts the binding of PilM to PilB, PilT, and PilC. Based on these analyses, we predict that the binding of PilN to PilM dynamically regulates PilM binding to PilB, PilT, and/or PilC

(Fig. 7). One hypothesis might be that PilN detachment from PilM is part of a molecular switch regulating a T4aP process, such as extension or retraction. The newly identified protein-protein interactions described herein suggest that PilM is not simply a passive scaffold but potentially a key regulator of T4aP dynamics.

Author Contributions—M. M. performed all experiments and wrote the manuscript. S. T. aided in experimental design and edited the manuscript. J. K. performed the EM studies. D. J. L. aided with crystal screening, structure solution, and crystallographic data analysis and edited the manuscript. H. R. collected crystallographic data at the X29 beamline. M. S., C. C., and T. F. M. performed SEC-MALS analysis. M. M., L. L. B., and P. L. H. designed the project, analyzed the results, and wrote the manuscript. All authors reviewed and approved the final version of this article.

Acknowledgments—We thank Patrick Yip for technical assistance and Liliana Sampaleanu, Ryan Buensuceso, Tiffany Leighton, Hanjeong Harvey, and Daniel Yong for generation of initial PilM vectors and several BACTH constructs and for helpful discussions. Beamline X29 at the National Synchrotron Light Source, Brookhaven National Laboratory, is supported by the Department of Energy and by a grant from the National Institutes of Health National Center for Research Resources. Funds for the x-ray facilities at the Hospital for Sick Children were provided, in part, by the Canadian Foundation for Innovation.

References

1. Luo, Y., Zhao, K., Baker, A. E., Kuchma, S. L., Coggan, K. A., Wolfgang, M. C., Wong, G. C., and O'Toole, G. A. (2015) A hierarchical cascade of second messengers regulates *Pseudomonas aeruginosa* surface behaviors. *MBio* 10.1128/mBio.02456-14
2. Chiang, P., and Burrows, L. L. (2003) Biofilm formation by hyperpiliated mutants of *Pseudomonas aeruginosa*. *J. Bacteriol.* **185,** 2374–2378
3. Burrows, L. L. (2012) Pseudomonas aeruginosa twitching motility: type IV pili in action. *Annu. Rev. Microbiol.* **66,** 493–520
4. Conrad, J. C., Gibiansky, M. L., Jin, F., Gordon, V. D., Motto, D. A., Mathewson, M. A., Stopka, W. G., Zelasko, D. C., Shrout, J. D., and Wong, G. C. (2011) Flagella and pili-mediated near-surface single-cell motility mechanisms in *P. aeruginosa*. *Biophys. J.* **100,** 1608–1616
5. Anyan, M. E., Amiri, A., Harvey, C. W., Tierra, G., Morales-Soto, N., Driscoll, C. M., Alber, M. S., and Shrout, J. D. (2014) Type IV pili interactions promote intercellular association and moderate swarming of *Pseudomonas aeruginosa*. *Proc. Natl. Acad. Sci. U.S.A.* **111,** 18013–18018
6. Chen, I., and Dubnau, D. (2004) DNA uptake during bacterial transformation. *Nat. Rev. Microbiol.* **2,** 241–249
7. Leighton, T. L., Buensuceso, R. N., Howell, P. L., and Burrows, L. L. (2015) Biogenesis of *Pseudomonas aeruginosa* type IV pili and regulation of their function. *Environ. Microbiol.* **17,** 4148–4163
8. Berry, J. L., and Pelicic, V. (2015) Exceptionally widespread nanomachines composed of type IV pilins: the prokaryotic Swiss Army knives. *FEMS Microbiol. Rev.* **39,** 134–154
9. Stephanie Tammam, P. Lynne Howell, and Burrows, L. L. (2014) in *Bacterial Pili: Structure, Synthesis, and Role in Disease* (Barocchi, M. A., and Telford, J. L., eds) pp. 85–99, Novartis Vaccines and Diagnostics, Siena, Italy
10. Chiang, P., Sampaleanu, L. M., Ayers, M., Pahuta, M., Howell, P. L., and Burrows, L. L. (2008) Functional role of conserved residues in the characteristic secretion NTPase motifs of the *Pseudomonas aeruginosa* type IV pilus motor proteins PilB, PilT and PilU. *Microbiology* **154,** 114–126
11. Merz, A. J., So, M., and Sheetz, M. P. (2000) Pilus retraction powers bacterial twitching motility. *Nature* **407,** 98–102
12. Whitchurch, C. B., Hobbs, M., Livingston, S. P., Krishnapillai, V., and Mattick, J. S. (1991) Characterisation of a *Pseudomonas aeruginosa* twitching motility gene and evidence for a specialised protein export system widespread in eubacteria. *Gene* **101,** 33–44
13. Wolfgang, M., van Putten, J. P., Hayes, S. F., Dorward, D., and Koomey, M. (2000) Components and dynamics of fiber formation define a ubiquitous biogenesis pathway for bacterial pili. *EMBO J.* **19,** 6408–6418
14. Tammam, S., Sampaleanu, L. M., Koo, J., Manoharan, K., Daubaras, M., Burrows, L. L., and Howell, P. L. (2013) PilMNOPQ from the *Pseudomonas aeruginosa* type IV pilus system form a transenvelope protein interaction network that interacts with PilA. *J. Bacteriol.* **195,** 2126–2135
15. Karuppiah, V., and Derrick, J. P. (2011) Structure of the PilM-PilN inner membrane type IV pilus biogenesis complex from *Thermus thermophilus*. *J. Biol. Chem.* **286,** 24434–24442
16. Ayers, M., Sampaleanu, L. M., Tammam, S., Koo, J., Harvey, H., Howell, P. L., and Burrows, L. L. (2009) PilM/N/O/P proteins form an inner membrane complex that affects the stability of the *Pseudomonas aeruginosa* type IV pilus secretin. *J. Mol. Biol.* **394,** 128–142
17. Takhar, H. K., Kemp, K., Kim, M., Howell, P. L., and Burrows, L. L. (2013) The platform protein is essential for type IV pilus biogenesis. *J. Biol. Chem.* **288,** 9721–9728
18. Jacobs, M. A., Alwood, A., Thaipisuttikul, I., Spencer, D., Haugen, E., Ernst, S., Will, O., Kaul, R., Raymond, C., Levy, R., Chun-Rong, L., Guenthner, D., Bovee, D., Olson, M. V., and Manoil, C. (2003) Comprehensive transposon mutant library of *Pseudomonas aeruginosa*. *Proc. Natl. Acad. Sci. U.S.A.* **100,** 14339–14344
19. Martin, P. R., Watson, A. A., McCaul, T. F., and Mattick, J. S. (1995) Characterization of a five-gene cluster required for the biogenesis of type 4 fimbriae in *Pseudomonas aeruginosa*. *Mol. Microbiol.* **16,** 497–508
20. Bahar, O., Goffer, T., and Burdman, S. (2009) Type IV Pili are required for virulence, twitching motility, and biofilm formation of *acidovorax avenae* subsp. *Citrulli*. *Mol. Plant. Microbe Interact.* **22,** 909–920
21. Roine, E., Nunn, D. N., Paulin, L., and Romantschuk, M. (1996) Characterization of genes required for pilus expression in *Pseudomonas syringae* pathovar *phaseolicola*. *J. Bacteriol.* **178,** 410–417
22. Carbonnelle, E., Helaine, S., Nassif, X., and Pelicic, V. (2006) A systematic genetic analysis in *Neisseria meningitidis* defines the Pil proteins required for assembly, functionality, stabilization and export of type IV pili. *Mol. Microbiol.* **61,** 1510–1522
23. Rumszauer, J., Schwarzenlander, C., and Averhoff, B. (2006) Identification, subcellular localization and functional interactions of PilMNOWQ and PilA4 involved in transformation competency and pilus biogenesis in the thermophilic bacterium *Thermus thermophilus* HB27. *FEBS J.* **273,** 3261–3272
24. Yamagata, A., Milgotina, E., Scanlon, K., Craig, L., Tainer, J. A., and Donnenberg, M. S. (2012) Structure of an essential type IV pilus biogenesis protein provides insights into pilus and type II secretion systems. *J. Mol. Biol.* **419,** 110–124
25. Sandkvist, M., Bagdasarian, M., and Howard, S. P. (2000) Characterization of the multimeric Eps complex required for cholera toxin secretion. *Int. J. Med. Microbiol.* **290,** 345–350
26. Camberg, J. L., Johnson, T. L., Patrick, M., Abendroth, J., Hol, W. G., and Sandkvist, M. (2007) Synergistic stimulation of EpsE ATP hydrolysis by EpsL and acidic phospholipids. *EMBO J.* **26,** 19–27
27. Py, B., Loiseau, L., and Barras, F. (2001) An inner membrane platform in the type II secretion machinery of Gram-negative bacteria. *EMBO Rep.* **2,** 244–248
28. Lu, C., Korotkov, K. V., and Hol, W. G. (2014) Crystal structure of the full-length ATPase GspE from the *Vibrio vulnificus* type II secretion system in complex with the cytoplasmic domain of GspL. *J. Struct. Biol.* **187,** 223–235
29. van den Ent, F., Amos, L. A., and Löwe, J. (2001) Prokaryotic origin of the actin cytoskeleton. *Nature* **413,** 39–44
30. Szwedziak, P., Wang, Q., Freund, S. M., and Löwe, J. (2012) FtsA forms actin-like protofilaments. *EMBO J.* **31,** 2249–2260
31. Tsang, M. J., and Bernhardt, T. G. (2015) Guiding divisome assembly and controlling its activity. *Curr. Opin. Microbiol.* **24,** 60–65
32. Pichoff, S., Du, S., and Lutkenhaus, J. (2015) The bypass of ZipA by overexpression of FtsN requires a previously unknown conserved FtsN motif

essential for FtsA-FtsN interaction supporting a model in which FtsA monomers recruit late cell division proteins to the Z ring. *Mol. Microbiol.* **95,** 971–987
33. Busiek, K. K., Eraso, J. M., Wang, Y., and Margolin, W. (2012) The early divisome protein FtsA interacts directly through its 1c subdomain with the cytoplasmic domain of the late divisome protein FtsN. *J. Bacteriol.* **194,** 1989–2000
34. Szwedziak, P., and Löwe, J. (2013) Do the divisome and elongasome share a common evolutionary past? *Curr. Opin. Microbiol.* **16,** 745–751
35. Lee, J. E., Cornell, K. A., Riscoe, M. K., and Howell, P. L. (2001) Structure of *E. coli* 5′-methylthioadenosine/S-adenosylhomocysteine nucleosidase reveals similarity to the purine nucleoside phosphorylases. *Structure* **9,** 941–953
36. Otwinowski, Z., and Minor, W. (1997) Processing of x-ray diffraction data collected in oscillation mode. *Methods Enzymol.* **276,** 307–326
37. Chen, V. B., Arendall, W. B., 3rd, Headd, J. J., Keedy, D. A., Immormino, R. M., Kapral, G. J., Murray, L. W., Richardson, J. S., and Richardson, D. C. (2010) MolProbity: all-atom structure validation for macromolecular crystallography. *Acta Crystallogr. D Biol. Crystallogr.* **66,** 12–21
38. Terwilliger, T. C., Adams, P. D., Read, R. J., McCoy, A. J., Moriarty, N. W., Grosse-Kunstleve, R. W., Afonine, P. V., Zwart, P. H., and Hung, L. W. (2009) Decision-making in structure solution using Bayesian estimates of map quality: the PHENIX AutoSol wizard. *Acta Crystallogr. D Biol. Crystallogr.* **65,** 582–601
39. Zwart, P. H., Afonine, P. V., Grosse-Kunstleve, R. W., Hung, L. W., Ioerger, T. R., McCoy, A. J., McKee, E., Moriarty, N. W., Read, R. J., Sacchettini, J. C., Sauter, N. K., Storoni, L. C., Terwilliger, T. C., and Adams, P. D. (2008) Automated structure solution with the PHENIX suite. *Methods Mol. Biol.* **426,** 419–435
40. Emsley, P., Lohkamp, B., Scott, W. G., and Cowtan, K. (2010) Features and development of Coot. *Acta Crystallogr. D Biol. Crystallogr.* **66,** 486–501
41. McCoy, A. J., Grosse-Kunstleve, R. W., Adams, P. D., Winn, M. D., Storoni, L. C., and Read, R. J. (2007) Phaser crystallographic software. *J. Appl. Crystallogr.* **40,** 658–674
42. Adams, P. D., Afonine, P. V., Bunkóczi, G., Chen, V. B., Davis, I. W., Echols, N., Headd, J. J., Hung, L. W., Kapral, G. J., Grosse-Kunstleve, R. W., McCoy, A. J., Moriarty, N. W., Oeffner, R., Read, R. J., Richardson, D. C., et al. (2010) PHENIX: a comprehensive Python-based system for macromolecular structure solution. *Acta Crystallogr. D Biol. Crystallogr.* **66,** 213–221
43. Feng, J., Chen, Y., Pu, J., Yang, X., Zhang, C., Zhu, S., Zhao, Y., Yuan, Y., Yuan, H., and Liao, F. (2011) An improved malachite green assay of phosphate: mechanism and application. *Anal. Biochem.* **409,** 144–149
44. Gish, W., and States, D. J. (1993) Identification of protein coding regions by database similarity search. *Nat. Genet.* **3,** 266–272
45. Tamura, K., Peterson, D., Peterson, N., Stecher, G., Nei, M., and Kumar, S. (2011) MEGA5: molecular evolutionary genetics analysis using maximum likelihood, evolutionary distance, and maximum parsimony methods. *Mol. Biol. Evol.* **28,** 2731–2739
46. Stothard, P. (2000) The sequence manipulation suite: JavaScript programs for analyzing and formatting protein and DNA sequences. *BioTechniques* **28,** 1102–1104
47. Crooks, G. E., Hon, G., Chandonia, J. M., and Brenner, S. E. (2004) WebLogo: a sequence logo generator. *Genome Res.* **14,** 1188–1190
48. Battesti, A., and Bouveret, E. (2012) The bacterial two-hybrid system based on adenylate cyclase reconstitution in *Escherichia coli*. *Methods* **58,** 325–334
49. Karimova, G., Pidoux, J., Ullmann, A., and Ladant, D. (1998) A bacterial two-hybrid system based on a reconstituted signal transduction pathway. *Proc. Natl. Acad. Sci. U.S.A.* **95,** 5752–5756
50. Leighton, T. L., Dayalani, N., Sampaleanu, L. M., Howell, P. L., and Burrows, L. L. (2015) A novel role for PilNO in type IV pilus retraction revealed by alignment subcomplex mutations. *J. Bacteriol.* **197,** 2229–2238
51. Abendroth, J., Murphy, P., Sandkvist, M., Bagdasarian, M., and Hol, W. G. (2005) The x-ray structure of the type II secretion system complex formed by the N-terminal domain of EpsE and the cytoplasmic domain of EpsL of *Vibrio cholerae*. *J. Mol. Biol.* **348,** 845–855
52. Krissinel, E., and Henrick, K. (2007) Inference of macromolecular assemblies from crystalline state. *J. Mol. Biol.* **372,** 774–797
53. Dominguez, R. (2000) A common binding site for actin-binding proteins on the actin surface. in *Madame Curie Bioscience Database*, Landes Bioscience, Austin, TX
54. Day, E. S., Cote, S. M., and Whitty, A. (2012) Binding efficiency of protein-protein complexes. *Biochemistry* **51,** 9124–9136
55. Mayer, M. P. (2013) Hsp70 chaperone dynamics and molecular mechanism. *Trends Biochem. Sci.* **38,** 507–514
56. Taylor, D., Cawley, G., and Hayward, S. (2014) Quantitative method for the assignment of hinge and shear mechanism in protein domain movements. *Bioinformatics* **30,** 3189–3196
57. Karimova, G., Ullmann, A., and Ladant, D. (2000) *Bordetella pertussis* adenylate cyclase toxin as a tool to analyze molecular interactions in a bacterial two-hybrid system. *Int. J. Med. Microbiol.* **290,** 441–445
58. Georgiadou, M., Castagnini, M., Karimova, G., Ladant, D., and Pelicic, V. (2012) Large-scale study of the interactions between proteins involved in type IV pilus biology in *Neisseria meningitidis*: characterization of a subcomplex involved in pilus assembly. *Mol. Microbiol.* **84,** 857–873
59. Pichoff, S., and Lutkenhaus, J. (2005) Tethering the Z ring to the membrane through a conserved membrane targeting sequence in FtsA. *Mol. Microbiol.* **55,** 1722–1734
60. Salje, J., van den Ent, F., de Boer, P., and Löwe, J. (2011) Direct membrane binding by bacterial actin MreB. *Mol. Cell* **43,** 478–487
61. Krupka, M., Cabré, E. J., Jiménez, M., Rivas, G., Rico, A. I., and Vicente, M. (2014) Role of the FtsA C terminus as a switch for polymerization and membrane association. *MBio* **5,** e02221
62. Holmes, K. C., Sander, C., and Valencia, A. (1993) A new ATP-binding fold in actin, hexokinase and Hsc70. *Trends Cell Biol.* **3,** 53–59
63. Swain, J. F., Dinler, G., Sivendran, R., Montgomery, D. L., Stotz, M., and Gierasch, L. M. (2007) Hsp70 chaperone ligands control domain association via an allosteric mechanism mediated by the interdomain linker. *Mol. Cell* **26,** 27–39
64. Barthel, T. K., Zhang, J., and Walker, G. C. (2001) ATPase-defective derivatives of *Escherichia coli* DnaK that behave differently with respect to ATP-induced conformational change and peptide release. *J. Bacteriol.* **183,** 5482–5490
65. Skerker, J. M., and Berg, H. C. (2001) Direct observation of extension and retraction of type IV pili. *Proc. Natl. Acad. Sci. U.S.A.* **98,** 6901–6904
66. Touhami, A., Jericho, M. H., Boyd, J. M., and Beveridge, T. J. (2006) Nanoscale characterization and determination of adhesion forces of *Pseudomonas aeruginosa* pili by using atomic force microscopy. *J. Bacteriol.* **188,** 370–377
67. Bischof, L. F., Friedrich, C., Harms, A., Søgaard-Andersen, L., and van der Does, C. (2016) The type IV pilus assembly ATPase PilB of *Myxococcus xanthus* interacts with the inner membrane platform protein PilC and the nucleotide binding protein PilM. *J. Biol. Chem.* **291,** 6946–6957
68. Brown, P., Pullan, W., Yang, Y., and Zhou, Y. (2016) Fast and accurate non-sequential protein structure alignment using a new asymmetric linear sum assignment heuristic. *Bioinformatics* **32,** 370–377
69. Karplus, P. A., and Diederichs, K. (2012) Linking crystallographic model and data quality. *Science* **336,** 1030–1033